13 Hedin Equations, *GW, GW*+DMFT, and All That

K. Held, C. Taranto, G. Rohringer, and A. Toschi
Institute for Solid State Physics
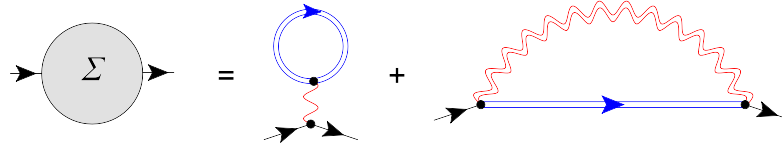Vienna University of Technology, 1040 Vienna, Austria

Contents

Fig. 1: *In GW, the self energy is given by the Hartree term plus a Fock-like term which is however in terms of the screened Coulomb interaction W (double wiggled line) instead of the bare Coulomb interaction V (single wiggled line). The interacting Green function G is denoted by a double straight line.*

1   Introduction

An alternative to density functional theory [1–3] for calculating materials *ab initio* is the so-called GW approach [4, 5]. The name stems from the way the self energy is calculated in this approach: It is given by the product of the Green function G and the screened Coulomb interaction W, see Fig. 1:

$$\Sigma^{\mathrm{GW}}(\mathbf{r}, \mathbf{r}'; \omega) = i \int \frac{d\omega'}{2\pi} G(\mathbf{r}, \mathbf{r}'; \omega + \omega') W(\mathbf{r}, \mathbf{r}'; \omega') . \tag{1}$$

This self energy contribution supplements the standard Hartree term (first diagram in Fig. 1.) Here, $\mathbf{r}$ and $\mathbf{r}'$ denote two positions in real space, ω the frequency of interest; and the imaginary unit i in front of G stems from the standard definition of the real time (or real frequency) Green function and the rules for evaluating the diagram Fig. 1, see e.g. [6].

In GW, the screened Coulomb interaction W is calculated within the random phase approximation (RPA) [7]. That is, the screening is given by the (repeated) interaction with independent electron-hole pairs, see Fig. 2. For example, the physical interpretation of the second diagram in the second line of Fig. 2 is as follows: two electrons do not interact directly with each other as in the first term (bare Coulomb interaction) but the interaction is mediated via a virtual electron-hole pair (Green function bubble). Also included are repeated screening processes of this kind (third term etc.). Because of the virtual particle-hole pair(s), charge is redistributed dynamically, and the electrons only see the other electrons through a screened interaction. Since this RPA-screening is a very important contribution from the physical point of view and since, at the same time, it is difficult to go beyond, one often restricts oneself to this approximation when considering screening, as it is done in GW.

For visualizing what kind of electronic correlations are included in the GW approach, we can replace the screened interaction in Fig. 1 by its RPA expansion Fig. 2. This generates the Feynman diagrams of Fig. 3. We see that besides the Hartree and Fock term (first line), additional diagrams emerge (second line). By the definition that correlations are *what goes beyond Hartree-Fock*, these diagrams constitute the electronic correlations of the GW approximation. They give rise to quasiparticle renormalizations and finite quasiparticle lifetimes as well as to renormalizations of the gaps in band insulators or semiconductors.

It is quite obvious that a restriction of the electronic correlations to only the second line of Fig. 3 is not sufficient if electronic correlations are truly strong such as in transition metal

Fig. 2: *The screened interaction W (double wiggled line) is calculated from the bare Coulomb interaction V (single wiggled line) and corrections which describe screening processes. In GW, the screening is given by the random phase approximation, i.e., only bubble diagrams in a geometric series (second line) are considered. This geometric series can be generated from a single bubble connected to the screened interaction (first line). If we start with $W = V$ on the right hand side of the first line, we will generate the second term of the second line, and by further iterations obtain the whole series (whole second line).*

Fig. 3: *Substituting the screened interaction of Fig. 2 into the self energy diagram Fig. 1 generates besides the Hartree term (which is independently considered) the Fock term (first line), and some electronic correlations beyond (second line).*

oxides or f-electron systems. The GW approximation cannot describe Hubbard side bands or Mott-Hubbard metal-insulator transitions. Its strength is for weakly correlated electron systems and, in particular, for semiconductors. For these, extended sp^3 orbitals lead to an important contribution of the non-local exchange. This is not well included (underrated) in the local exchange-correlation potential V_{xc} of the local density approximation (LDA) and overrated by the bare Fock term. The GW exchange is "in between" in magnitude and energy dependence, which is also important, as we will see later. If it is, instead, the local correlation-part of V_{xc} which needs to be improved upon, as in the aforementioned transition metal oxides or f-electron systems, we need to employ dynamical mean field theory (DMFT) [8–10] or similar many-body approaches.

Historically, the GW approach was put forward by Hedin [4] as the simplest approximation to the so-called Hedin equations. In Section 2, we will derive these Hedin equations from a Feynman-diagrammatical point of view. Section 3.1 shows how GW arises as an approximation to the Hedin equations. In Section 3.2, we will briefly present some typical GW results for materials, including the aforementioned quasiparticle renormalizations, lifetimes, and band gap enhancements. In Section 4, the combination of GW and DMFT is summarized. Finally, as a prospective outlook, *ab initio* dynamical vertex approximation (DΓA) is introduced in Section 5 as a unifying scheme for all that: GW, DMFT and non-local vertex correlations beyond.

2   Hedin equations

In his seminal paper [4], Hedin noted, when deriving the equations bearing his name: "The results [i.e., the Hedin equations] are well known to the Green function people". And indeed, what is known as the Hedin equations in the bandstructure community are simply the Heisenberg equation of motion for the self energy (also known as Schwinger-Dyson equation) and the standard relations between irreducible and reducible vertex, self energy and Green function, polarization operator and screened interaction. While Hedin gave an elementary derivation with only second quantization as a prerequisite, we will discuss these from a Feynman diagrammatic point of view as the reader/student shall by now be familiar with this technique from the previous chapters/lectures of the Summer School. Our point of view gives a complementary perspective and sheds some light to the relation to standard many body theory. For Hedin's elementary derivation based on functional derivatives see [4] and [5].

Let us start with the arguably simplest **Hedin equation**: the well known *Dyson equation*, Fig. 4, which connects self energy and Green function:

$$
\begin{aligned}
G(11') &= G^0(11') + G(12)\beta\Sigma(22')G^0(2'1') \\
&= G^0(11') + G^0(12)\beta\Sigma(22')G^0(2'1') + G^0(13)\beta\Sigma(33')G^0(3'2)\beta\Sigma(22')G^0(2'1') + \dots
\end{aligned}
\tag{2}
$$

Here, we have introduced a short-hand notation with 1 representing a space-time coordinate $(\mathbf{r}_1, \tau_1)$ also subsuming a spin if present; employ Einstein summation convention; G and G^0 denote the interacting and non-interacting ($V = 0$) Green function[1], respectively. Here and in the following part of this Section we will consider the Green function in imaginary time with Wick rotation $t \to -i\tau$, and closely follow the notation of [11][2].

In terms of Feynman diagrams, the Dyson equation means that we collect all one-particle *irreducible* diagrams, i.e., all diagrams that do not fall apart into two pieces if one Green function line is cut, and call this object Σ. All Feynman diagrams for the interacting Green function are then generated simply by connecting the one-particle irreducible building blocks Σ by Green function lines in the Dyson equation (second line of Fig. 4). This way, no diagram is counted twice since all additional diagrams generated by the Dyson equation are one-particle *reducible* and hence not taken into account for a second time. On the other hand all diagrams are generated: the irreducible ones are already contained in Σ and the reducible ones have by definition

---

[1]Please recall the definition of the Green function with Wick time-ordering operator T for τ_1 and τ_1':

$$
\begin{aligned}
G(11') &\equiv -\langle \mathcal{T}c(1)c(1')^\dagger \rangle \ . \tag{3} \\
&\equiv -\langle \mathcal{T}c(1)c(1')^\dagger \rangle \Theta(\tau_1 - \tau_{1'}) + \langle \mathcal{T}c(1')^\dagger c(1) \rangle \Theta(\tau_{1'} - \tau_1) \tag{4}
\end{aligned}
$$

The first term of Eq. (4) describes the propagation of a particle from $1'$ to 1 (and the second line the corresponding propagation of a hole). Graphically we hence denote $G(11')$ by a straight line with an arrow from $1'$ to 1 (The reader might note the reverse oder in $G(11')$; we usually apply operators from right to left).

[2]Note that in [11] summations are defined as $(1/\beta)\int_0^\beta \mathrm{d}\tau$ or in Matsubara frequencies $\sum_m$; Fourier transformations are defined as $G(\tau) = \sum_m e^{-i\nu_m\tau}G(\nu_m)$. The advantage of this definition is that the equations have then the same form in τ and ν_m. Hence, we employ this notation in this Section and in Section 3. In Sections 1 and 4, the more standard definitions [6] are employed, i.e., $\int_0^\beta \mathrm{d}\tau$; $(1/\beta)\sum_m$. This results in some factors β (inverse temperatur), which can be ignored if one only wants to understand the equations.
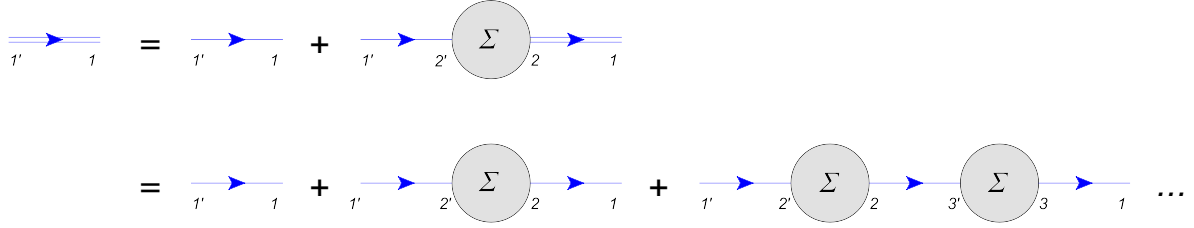
Fig. 4: *One of the five Hedin equations is the well-known Dyson equation, connecting the interacting Green function G (double line), non-interacting Green function G^0 (single line) and self energy Σ.*

the form of the second line of Fig. 4.

Let us note that the Dyson equation (2) can be resolved for

$$G(11') = \left(\left[\left(G^0\right)^{-1} - \beta \Sigma \right]^{-1} \right)_{(11')} \tag{5}$$

with a matrix inversion in the spatial and temporal coordinates. It is invariant under a basis transformation from $\mathbf{r}_1$ to, say, an orbital basis or from time to frequency (note in a momentum-frequency basis, the G and Σ matrices are diagonal).

A second equation of the five Hedin equations actually has the same form as the *Dyson equation* but with the Green function and interaction changing their role. It relates the *screened Coulomb interaction W* to the polarization operator P, see Fig. 5, which is a generalization of Fig. 2 to arbitrary polarizations. As W we simply define (sum) all Feynman diagrams which connect to the left and right side by interactions V. Physically, this means that we consider, besides the bare interaction, also all more complicated processes involving additional electrons (screening). Similar as for the Dyson equation (2), we collect all Feynman diagrams which do not fall apart into a *left* and a *right* side by cutting one *interaction line V*, and call this object P. From P, we can generate all diagrams of W connecting left and right side by a geometric series (second and third line of Fig. 5) with a repeated application of P and V (second line of Fig. 5). As for the Dyson equation, we generate all Feynman diagrams (in this case for W) and count none twice this way.

Mathematically, Fig. 5 translates into a **second Hedin equation**

$$W(11'; 22') = V(11'; 22') + W(11'; 33')P(3'3; 4'4)V(44'; 22') . \tag{6}$$

Note, that in a general basis the two particle objects have four indices: an incoming particle 2' and hole 2, and an outgoing particle 1' and hole 1, with possible four different orbital indices. In real space two of the indices are identical $\mathbf{r}_1 = \mathbf{r}_{1'}$ and $\mathbf{r}_2 = \mathbf{r}_{2'}$.[3]

Next, we turn to the polarization operator P which can be related to a vertex Γ^*. This is the standard relation between two particle Green functions (or response functions) and the vertex

---

[3] This is obvious for the bare Coulomb interaction $V(\mathbf{r}_1, \mathbf{r}_1'; \mathbf{r}_2, \mathbf{r}_2') = V(\mathbf{r}_1, \mathbf{r}_2)\delta(\mathbf{r}_1 - \mathbf{r}_1')\delta(\mathbf{r}_2 - \mathbf{r}_2')$ with $V(\mathbf{r}_1, \mathbf{r}_2) = \frac{e^2}{4\pi\epsilon_0} \frac{1}{|\mathbf{r}_1 - \mathbf{r}_2|}$. As one can see in Fig. 5 this property is transfered to W for which hence only a polarization with two $\mathbf{r}$'s needs to be calculated in real space.

Fig. 5: *A second of the five Hedin equations is an ananlogon of the Dyson equation, Fig. 4 but for the Coulomb interaction. It relates the screened Coulomb interaction W (double wiggled line) with the bare Coulomb interaction V and the polarization operator P. As the Dyson equation can be considered as the defining equation for Σ, this second Hedin equation effectively defines what P is.*

Fig. 6: *A third Hedin equation relates the polarization operator P to two separated Green functions ("bubble" term) plus vertex (Γ^*) corrections. This is the standard relation between two particle Green functions and fully reducible vertex Γ. However since the polarization operator cannot include interaction-reducible diagrams Γ has to be replaced by Γ^* (see text). Second line: In terms of real space or momentum (but not in an orbital representation) two indices can be contracted to a single one (cf. footnote 3).*

and represents a **third Hedin equation**. That is P is given by the simple connection of left and right side by two (separated) Green functions plus vertex corrections, see Fig. 6:

$$P(11'; 22') = \beta G(12')G(21') + \beta G(13)G(3'1')\Gamma^*(33'; 44')\beta G(4'2')G(24) . \qquad (7)$$

Note, in real space $2 = 2'$ and $1 = 1'$ (cf. footnote 3) so that working with a two index object, see second line of Fig. 6, is possible (and was done by Hedin), the inverse temperature β ($k_B \equiv 1$) arises from the rules for Feynman diagrams in imaginary times/frequencies, see [11]. Let us keep in mind, that in P or Γ^* not all Feynman diagrams are included: those diagrams, that can be separated into left and right by cutting a single interaction line have to be explicitly excluded, see Fig. 7. This is the reason why we put the symbol * to the vertex Γ^*; indicating that some diagrams of the full vertex Γ are missing.

Having introduced the two-particle vertex Γ^*, the **fourth Hedin equation** is obtained by relating this vertex to another object, the particle-hole irreducible vertex Γ^*_{ph}. This relation is the
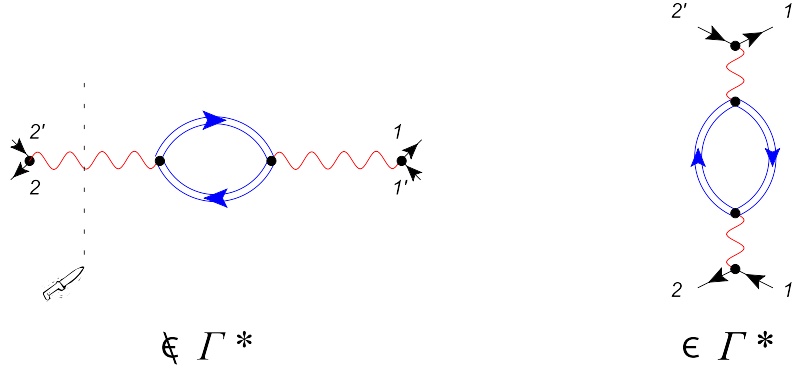
Fig. 7: *Left: A Feynman diagram that is **not** part of Γ^* (or P) since cutting a single interaction line separates the diagram into left and right part. Right: This Feynman diagram is included in Γ^* (or P).*
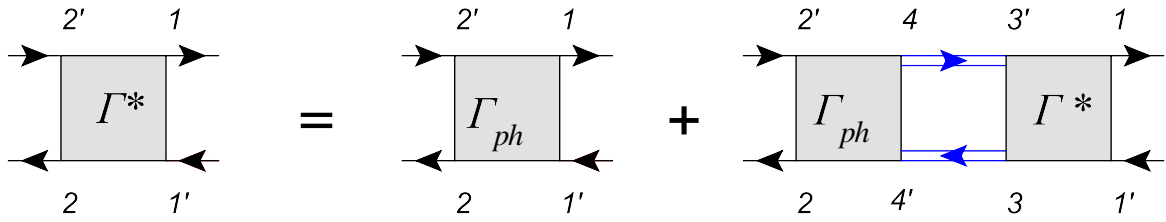

Fig. 8: *A fourth Hedin equation is the Bethe-Salpeter equation between the irreducible Γ^*_{ph} and particle-hole reducible vertex Γ^*. The particle-hole irreducible vertex Γ^*_{ph} collects the Feynman diagrams which cannot be separated into left and right part by cutting two Green function lines. All diagrams are then generated by the Bethe-Salpeter equation.*

standard Bethe-Salpeter equation. As in the Dyson equation, we define the vertex Γ^* as the irreducible vertex Γ^*_{ph} plus a geometric series of repetitions of Γ^*_{ph} connected by two Green functions, see Fig. 8:

$$\Gamma^*(11';22') = \Gamma^*_{\mathrm{ph}}(11';22') + \Gamma^*(11';33')\beta G(3'4)G(4'3)\Gamma^*_{\mathrm{ph}}(44';22') \tag{8}$$

Here, the particle-hole irreducible vertex collects all Feynman diagrams which cannot be separated by cutting *two* Green function lines into a left and right (incoming and outgoing) part. The Bethe-Salpeter equation then generates all vertex diagrams by connecting the irreducible building blocks with two Green function lines, in analogy to the Dyson equation for the one-particle irreducible vertex Σ.

Since in the polarization operator P (and the corresponding reducible vertex vertex Γ^*) diagrams which connect left and right by only one bare Coulomb interaction line V are however excluded, we have to explicitly take out this bare Coulomb interaction V from the vertex Γ^*, i.e., we have the standard particle-hole vertex Γ_{ph} (i.e., all particle-hole irreducible diagrams) minus the bare Coulomb interaction V diagram, see Fig. 9:

$$\Gamma^*_{\mathrm{ph}}(11';22') = \Gamma_{\mathrm{ph}}(11';22') - V(11';22') \tag{9}$$

The bare V and any combinations of Γ^*_{ph} and V are then generated in the screening equation (6), Fig. 5.
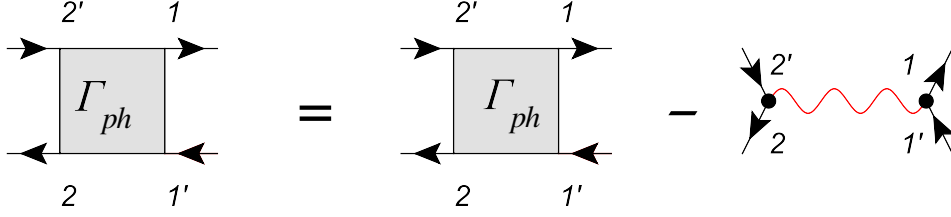
Fig. 9: *We have to exclude the bare Coulomb interaction V from the particle-hole vertex Γ_{ph} since such contributions are already considered in Fig. 5.*
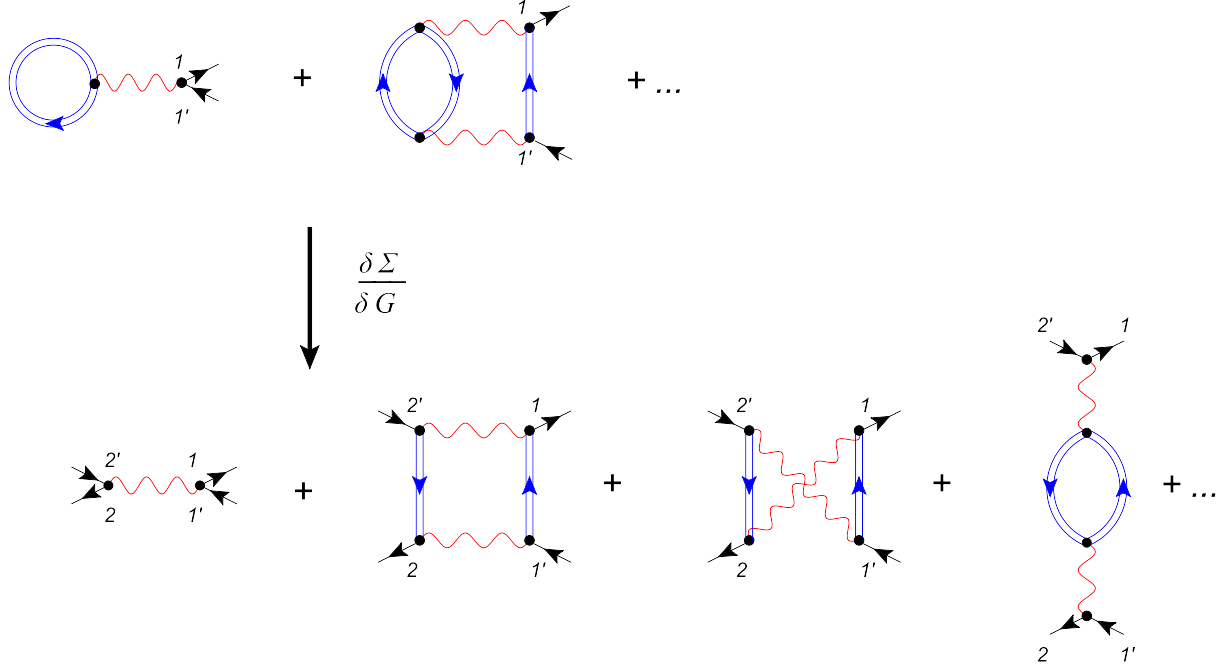
Fig. 10: *By hands of selected Feynman diagrams we illustrate that differentiation of Σ w.r.t. G yields the particle-hole irreducible vertex.*

In this fourth equation, Hedin directly expresses Γ_{ph}^* as the derivative of the self-energy w.r.t. the Green function [5] (respectively V [4]). This is a standard quantum field theoretical relation

$$\Gamma_{\mathrm{ph}}(11'; 22') = \frac{\delta\Sigma(11')}{\delta G(2'2)} \,, \tag{10}$$

which in terms of Feynman diagrams follows from the observation that differentiation w.r.t. G means removing one Green function line, see Fig. 10 and Ref. [11]. If we, as Hedin, consider the self energy without Hartree term $\Sigma_{\mathrm{Hartree}}(11') = V(11'; 22')G(2'2)$ we obtain the vertex Γ_{ph}^* instead of Γ_{ph}:

$$\Gamma_{\mathrm{ph}}^*(11'; 22') = \frac{\delta[\Sigma(11') - \Sigma_{\mathrm{Hartree}}(11')]}{\delta G(2'2)} \tag{11}$$

Note, the derivative of the Hartree term w.r.t. $G(2'2)$ yields $V(11'; 22')$, i.e., precisely the term not included in Γ_{ph}^*, see first diagram of Fig. 10.

The **fifth Hedin equation** is the *Heisenberg equation of motion* for the self energy, which follows from the derivative of the Green function (3) w.r.t. τ_1, i.e., the time-part of the coordinate

1. Let us start with the Heisenberg equation for the Heisenberg operator $c(1)$ ($\hbar \equiv 1$):

$$-\frac{\partial c(\mathbf{r}_1, \tau_1)}{\partial \tau_1} = [c(\mathbf{r}_1, \tau_1), H] \tag{12}$$

and a general Hamiltonian of the form

$$H = H_0(11')c(1)^\dagger c(1') + \frac{1}{2}V(11'; 22')c(1)^\dagger c(1')c(2)^\dagger c(2'). \tag{13}$$

From Eq. (12), we obtain the Heisenberg equation of motion for the Green function:[4]

$$-\frac{\partial G(11')}{\partial \tau_1} = \delta(1-1') + H_0(12')G(2'1') - V(13'; 22')\langle \mathcal{T}c(3')c(2)^\dagger c(2')c(1')^\dagger\rangle . \tag{14}$$

The last term on the right hand side of Eq. (14) is by definition the self energy times the Green function. Hence this combination equals the interaction V times a two-particle Green function. The two particle Green function in turn is, in analogy to Fig. 6, given by the bubble term (two Green function lines; there are actually two terms of this: crossed and non-crossed) and vertex correction with the full (reducible) vertex Γ. Besides the Hartree term, the self energy is given by (see Fig. 11):

$$\Sigma(11') = -V(13'; 22')\beta G(4'2)G(2'4)G(3'3)\Gamma(31'; 44') - V(12'; 21')G(2'2) \tag{15}$$

Note Eq. (15) can be formualted in an alternative way (see Appendix A for a detailed calculation): Instead of expressing this correlation part of the self energy by the bare interaction and the full vertex we can take out the bare interaction line V and any particle-hole repetitions of V from the vertex, i.e., take Γ^* instead of Γ. Consequently we need to replace V by W to generate the same set of all Feynman diagrams:

$$\Sigma(11') = -W(13'; 22')\beta G(4'2)G(2'4)G(3'3)\Gamma^*(31'; 44') - W(12'; 21')G(2'2) \tag{16}$$

see second line of Fig. 11.[5]

The five equations Eq. (2), (6), (7), (8), (16) correspond to Hedin's equations (A13), (A20), (A24), (A22), (A23), respectively [4] [or to equations (44), (46), (38), (45), and (43), respectively, in [5]). This set of equations is exact; it is equivalent to the text book quantum field

---

[4] Note, the first term here is generated by the time derivative of the Wick time ordering operator, the second term stems from $[c(1), H_0(22')c(2)^\dagger c(2')]$ and the third one from

$$[c(1), \frac{1}{2}V(33'; 22')c(3)^\dagger c(3')c(2)^\dagger c(2')]$$

employing $[A, BC] = B[A, C] + [A, B]C$ and the Fermi algebra $\{c(1'), c(1)^\dagger\} \equiv c(1')c(1)^\dagger + c(1)^\dagger c(1') = \delta(1-1'), \{c(1), c(1')\} = \{c(1)^\dagger, c(1')^\dagger\} = 0$.

[5] Note, Hedin defines as a "vertex" Λ [5] a combination of Γ^* and two Green function lines. Because he works in real space (or momentum) coordinates only at a common point $2 = 2'$ needs to be considered (in the same way as in the second line of Fig. 6). Hedin also adds a "1" in form of two δ-functions:

$$\Lambda(11'; 2) = \Gamma^*(11'; 33')\beta G(3'2)G(32) + \delta(1'-2)\delta(2-1) . \tag{17}$$
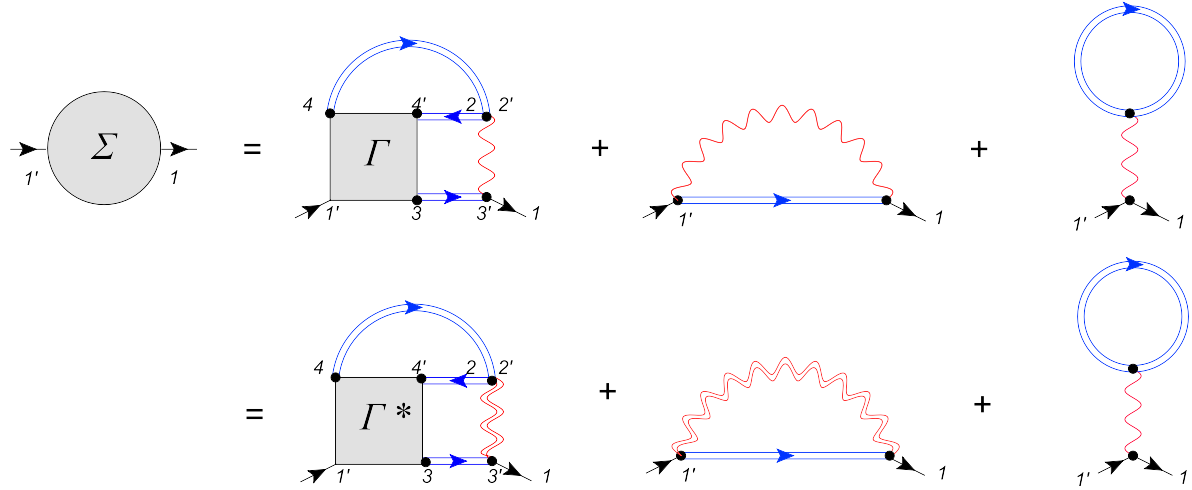
Fig. 11: *The fifth Hedin equation is the Heisenberg equation of motion, which connects the one-particle Green function with the two particle Green function or as shown in the figure (and as employed) the self energy with the vertex.*

theory [6, 11] relations between $\Gamma, \Gamma_{\text{ir}}$, Σ and G; but it contains additional equations since W and P are introduced. The advantage is that, this way, one can develop much more directly approximations where the screened Coulomb interaction plays a pronounced role such as in the GW approach.

3   *GW* approximation

3.1   From Hedin equations to *GW*

The simplest approximation is to neglect the vertex corrections completely, i.e., to set set $\Gamma_{\text{ph}}^* = 0$.[6] Then the Bethe-Salpeter equation (8) yields

$$\Gamma^* = 0 \ . \tag{18}$$

The polarization in Eq. (7) simplifies to the bubble

$$P^{\text{GW}}(11'; 22') = \beta G(12')G(21') \ . \tag{19}$$

The screened interaction in Eq. (6) is calculated with this simple polarization

$$W(11'; 22') = V(11'; 22') + W(11'; 33')P^{\text{GW}}(3'3; 4'4)V(44'; 22') \ . \tag{20}$$

The self energy in the Heisenberg equation of motion (16) simplifies to Fig. 2, i.e.,

$$\Sigma^{\text{GW}}(11') = -W(12'; 21')G(2'2) \tag{21}$$

(plus Hartree term).

From this, the Green function is obtained via the Dyson equation (2):

$$G(11') = G^0(11') + G(12)\beta\Sigma^{\text{GW}}(22')G^0(2'1') \tag{22}$$

These five (self-consistent) equations constitute the GW approximation.

---

[6]Note this violates the Pauli principle, see last paragraph of Appendix A.

3.2 *GW* band gaps and quasiparticles

While the five GW equations above are meant to be solved self-consistently, most calculations hitherto started from a LDA bandstructure calculation[7] and calculated from the LDA polarization (or dielectric constant) a screened interaction W_0 which in turn was used to determine the self energy with the Green function G_0 from the LDA: $\Sigma = iG_0W_0$.

Such calculations are already pretty reliable for semiconductor band gaps, which are underestimated in the LDA. Due to the energy(frequency)-dependence of Σ bands at different energies are under the influence of differently strong screened exchange contributions. In semiconductors, it turns out that the conduction band is shifted upwards in an approximately rigid way. The valence band is much less affected so that the GW band gap increases in comparison to the LDA gap. This effect can be mimicked by a so-called scissors operator, defined as cutting the density functional theory (DFT) bandstructure between valence and conduction band and moving the conduction band upwards. Cutting LDA bandstructures by a pair of scissors and rearranging them yields the GW bandstructure within an error of 0.1 eV for Si and 0.2 eV for GaAs [17].

More recently, self-consistent GW calculations became possible. Many of these calculations employ an approximation of Schilfgaarde and Kotani [18, 19] where instead of the frequency dependent GW self energy $\Sigma_{nn'}(\omega, \mathbf{q})$ a frequency-independent Hermitian operator

$$\bar{\Sigma}_{nn'} = \text{Re}[\Sigma_{nn'}(\epsilon_q, \mathbf{q}) + \Sigma_{n'n}(\epsilon_q, \mathbf{q})]/2 \tag{23}$$

is constructed in the basis n, n' employed in the GW/LDA algorithm. This self energy operator has the advantage that (as in LDA) we can remain in a one-particle description and employ the Kohn-Sham equations with Hermitian operator $\bar{\Sigma}_{nn'}$ to recalculate electron densities and Bloch eigenfunctions.

The band gaps of this self-consistent approach are slightly larger than experiment, see open triangles of Fig. 12. This can be improved upon and band gaps can be calculated very reliably if additional to GW (some) vertex corrections are taken into account. In Fig. 12, the inclusion of electron-hole ladder diagrams (visualized on the right hand side of Fig. 12) results in the filled triangles with band gaps being within a few percent of the experimental ones. As in other areas of many-body theory, doing the self-consistency without including vertex corrections does not seem to be an improvement w.r.t. the non-self-consistent GW since self-consistency and vertex corrections compensate each other in part. Full GW calculations beyond the Schilfgaarde and Kotani one-particle-ization (23) have only been started and applied to simple systems such as molecules [14, 13] and simple elements [15, 16].

Besides this big success to overcome a severe LDA/DFT shortcoming for semiconductor gaps, GW or G_0W_0 calculations also show a quasiparticle renormalization of the bandwidth. For alkali metals, electronic correlation are expected to be weak. Nonetheless experiments observe e.g. in Na a band narrowing (of the occupied bands) of 0.6 eV [22] compared to the nearly free electron theory. While GW [23] yields such a band narrowing, it is quantitatively with 0.3 eV

---

[7]An alternative, in particular for f electron systems, is to use LDA+U as a starting point [12].
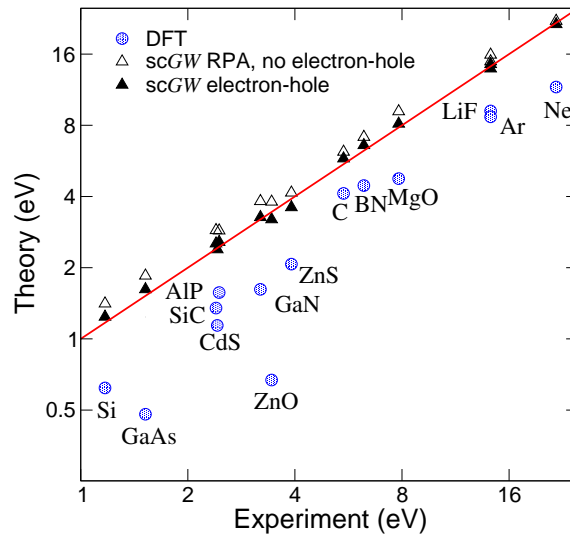
Fig. 12: *Theoretical vs. experimental band gap of DFT, self-consistent GW (scGW) without and with (some) vertex corrections (electron-hole ladder diagrams) (reproduced from [21]).*

only half as large as in experiment [23]. Of the more strongly correlated transition metals, Ni is best studied: here, the occupied d bandwidth is 1.2 eV smaller in experiment than LDA and there is a famous satellite peak at -6eV in the spectrum [24]. While GW [25] yields a band-narrowing of 1 eV which is surprisingly good (see Fig. 13), the satellite is missing. In fact, it can be identified as a (lower) Hubbard band whose description requires the inclusion of strong local correlation. This is possible by DMFT; and indeed the satellite is found in LDA+DMFT [26] and GW+DMFT calculations [27], see next section.

Besides the mentioned band-narrowing which is associated with a reduced quasiparticle weight or effective mass enhancement (related to the real part of the self energy), there is also the imaginary part of the GW self energy, which corresponds to a scattering rate. For Ag the GW scattering rate is reported to be in close agreement with the experimental one obtained from two-photon photoemission [28].

4   *GW*+DMFT

Since GW yields bandstructures similar to LDA (with the improvements for semiconductors discussed in the previous section) substituting the LDA part in LDA+DMFT by GW is very appealing from a theoretical point of view: Both approaches GW and DMFT are formulated in the same many-body framework, which does not only has the advantage of a more elegant combination, but also overcomes two fundamental problems of LDA+DMFT: (i) The screened Coulomb interaction employed for d-d or f-f interactions in DMFT can be straight forwardly calculated via W; one does not need an additional constrained LDA approximation [29–31] to this end; (ii) the double counting problem, i.e., to subtract the LDA/DFT contribution of the local d-d or f-f interaction which is included a second time in DMFT, can be addressed in a rigorous manner since for GW+DMFT we actually know which Feynman diagram is counted
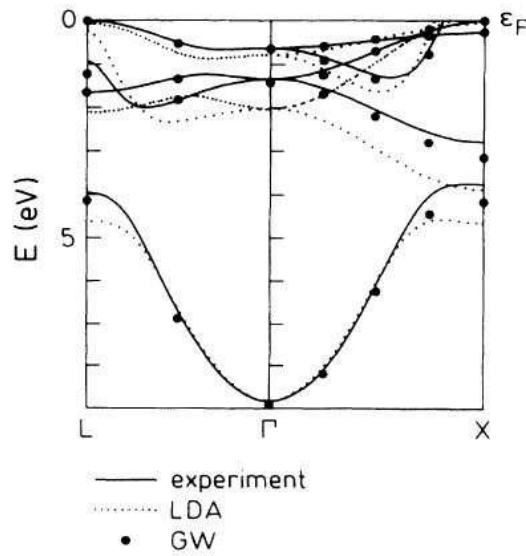
Fig. 13: *Experimental, LDA and GW bandstructure of Ni (reproduced from [25]).*
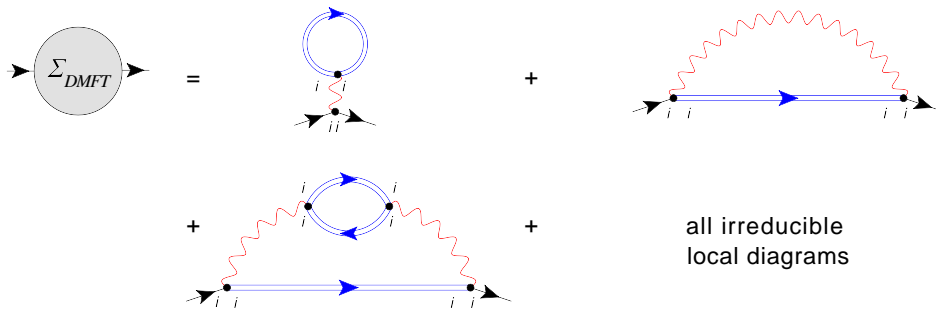
Fig. 14: *The DMFT self energy is calculated from the local contribution of all (one-particle irreducible) Feynman diagrams.*

twice.

Biermann *et al.* [27] proposed GW+DMFT, which they discuss from a functional integral point of view: a GW functional and a local impurity functional are added; the derivatives yield the mixed GW+DMFT equations. From a Feynman diagrammatic point of view, this corresponds to adding the GW self energy, Fig. 1 and the DMFT self energy which is just given by the local contribution of all (one-particle irreducible) Feynman diagrams, see Fig. 14. From these, the *local* screened exchange GW and the doubly counted Hartree term need obviously to be explicitly subtracted for not counting any diagram twice.

This results in the algorithm Fig. 15. Here, we leave the short-hand notation of Section 2 and 3.1 with $1, 2$ since GW is diagonal in ω and $\mathbf{k}$ and DMFT is diagonal in ω and site indices. Let us briefly discuss the GW+DMFT algorithm step-by-step; for more details see [32]:

- In most GW calculations, the starting point is a conventional LDA calculation (or another suitably chosen generalized Kohn-Sham calculation), yielding an electron density $\rho(\mathbf{r})$, bandstructure $\epsilon^{\mathrm{LDA}}(\mathbf{k})$ and also an LDA Green function $G_{\mathbf{k}}(\omega)$ (the latter is calculated as

Do LDA calculation, yielding $\boldsymbol{G_k}(\omega) = [\omega \mathbf{1} + \mu \mathbf{1} - \boldsymbol{\epsilon}^{\mathrm{LDA}}(\boldsymbol{k})]^{-1}$.

Calculate GW polarization $\boldsymbol{P}^{GW}(\omega) = -2i \int \frac{d\omega'}{2\pi} \boldsymbol{G}(\omega + \omega') \boldsymbol{G}(\omega')$.

If DMFT polarization $\boldsymbol{P}^{\mathrm{DMFT}}$ is known (after the 1st iteration), include it
$$\boldsymbol{P}^{GW\!+\!DMFT}(\boldsymbol{k}, \omega) = \boldsymbol{P}^{GW}(\boldsymbol{k}, \omega) - \frac{1}{V_{\mathrm{BZ}}} \int d^3 k \, \boldsymbol{P}^{GW}(\boldsymbol{k}, \omega) + \boldsymbol{P}^{\mathrm{DMFT}}(\omega) .$$

With this polarization, calculate the screened interaction:
$$\boldsymbol{W}(\boldsymbol{k}; \omega) = \boldsymbol{V}_{\mathrm{ee}}(\boldsymbol{k})[\mathbf{1} - \boldsymbol{V}_{\mathrm{ee}}(\boldsymbol{k}) \boldsymbol{P}(\boldsymbol{k}; \omega)]^{-1}.$$

Calculate $\boldsymbol{\Sigma}_{\boldsymbol{k}}^{\mathrm{Hartree}} = \int \frac{d^3 q}{V_{\mathrm{BZ}}} \boldsymbol{G}_{\boldsymbol{q}}(\tau = 0^-) \boldsymbol{W}(\boldsymbol{k} - \boldsymbol{q}, 0)$ and $\boldsymbol{\Sigma}_{\mathrm{dc}}^{\mathrm{Hartree}}$.

Calculate $\boldsymbol{\Sigma}^{GW}(\boldsymbol{r}, \boldsymbol{r}'; \omega) = i \int \frac{d\omega'}{2\pi} \boldsymbol{G}(\boldsymbol{r}, \boldsymbol{r}'; \omega + \omega') \boldsymbol{W}(\boldsymbol{r}, \boldsymbol{r}'; \omega')$.

Calculate the DMFT self-energy $\boldsymbol{\Sigma}^{\mathrm{DMFT}}$ and polarization $\boldsymbol{P}^{\mathrm{DMFT}}$ as follows:

From the local Green function $\boldsymbol{G}$ and old self-energy $\boldsymbol{\Sigma}^{\mathrm{DMFT}}$ calculate
$$(\boldsymbol{\mathcal{G}}^0)^{-1}(\omega) = \boldsymbol{G}^{-1}(\omega) + \boldsymbol{\Sigma}^{\mathrm{DMFT}}(\omega) \quad \boldsymbol{\Sigma}^{\mathrm{DMFT}} = 0 \text{ in 1st iteration.}$$

Extract the local screening contributions from $\boldsymbol{W}$:
$$\boldsymbol{U}(\omega) = [\boldsymbol{W}^{-1}(\omega) - \boldsymbol{P}^{\mathrm{DMFT}}(\omega)]^{-1}.$$

With $\boldsymbol{U}$ and $\boldsymbol{\mathcal{G}}^0$, solve impurity problem with effective action
$$\mathcal{A} = \sum_{\nu\sigma\,lm} \psi_{\nu m}^{\sigma*} (\mathcal{G}_{\nu mn}^{\sigma 0})^{-1} \psi_{\nu n}^{\sigma} + \sum_{lm\sigma\sigma'} \int d\tau \psi_l^{\sigma*}(\tau) \psi_l^{\sigma}(\tau) U_{lm}(\tau - \tau') \psi_m^{\sigma'*}(\tau') \psi_m^{\sigma'}(\tau'),$$
resulting in $\boldsymbol{G}$ and susceptibility $\boldsymbol{\chi}$.

From $\boldsymbol{G}$ and $\boldsymbol{\chi}$, calculate $\boldsymbol{\Sigma}^{\mathrm{DMFT}}(\omega) = (\boldsymbol{\mathcal{G}}^0)^{-1}(\omega) - \boldsymbol{G}^{-1}(\omega)$,
$\boldsymbol{P}^{\mathrm{DMFT}}(\omega) = \boldsymbol{U}^{-1}(\omega) - [\boldsymbol{U} - \boldsymbol{U}\boldsymbol{\chi}\boldsymbol{U}]^{-1}(\omega)$.

Combine this to the total GW self-energy:
$\boldsymbol{\Sigma}^{GW\!+\!DMFT}(\boldsymbol{k}, \omega) = \boldsymbol{\Sigma}^{GW}(\boldsymbol{k}, \omega) - \int d^3 k \, \boldsymbol{\Sigma}^{GW}(\boldsymbol{k}, \omega) + \boldsymbol{\Sigma}^{\mathrm{Hartree}}(\boldsymbol{k}) - \boldsymbol{\Sigma}_{\mathrm{dc}}^{\mathrm{Hartree}} + \boldsymbol{\Sigma}^{\mathrm{DMFT}}(\omega)$.

From this and $\boldsymbol{G}^0$, calculate $\boldsymbol{G}_{\boldsymbol{k}}^{\mathrm{new}}(\omega)^{-1} = \boldsymbol{G}_{\boldsymbol{k}}^0(\omega)^{-1} - \boldsymbol{\Sigma}_{\boldsymbol{k}}(\omega)$.

Iterate with $\boldsymbol{G}_{\boldsymbol{k}} = \boldsymbol{G}_{\boldsymbol{k}}^{\mathrm{new}}$ until convergence, i.e. $\|\boldsymbol{G}_{\boldsymbol{k}} - \boldsymbol{G}_{\boldsymbol{k}}^{\mathrm{new}}\| < \epsilon$.
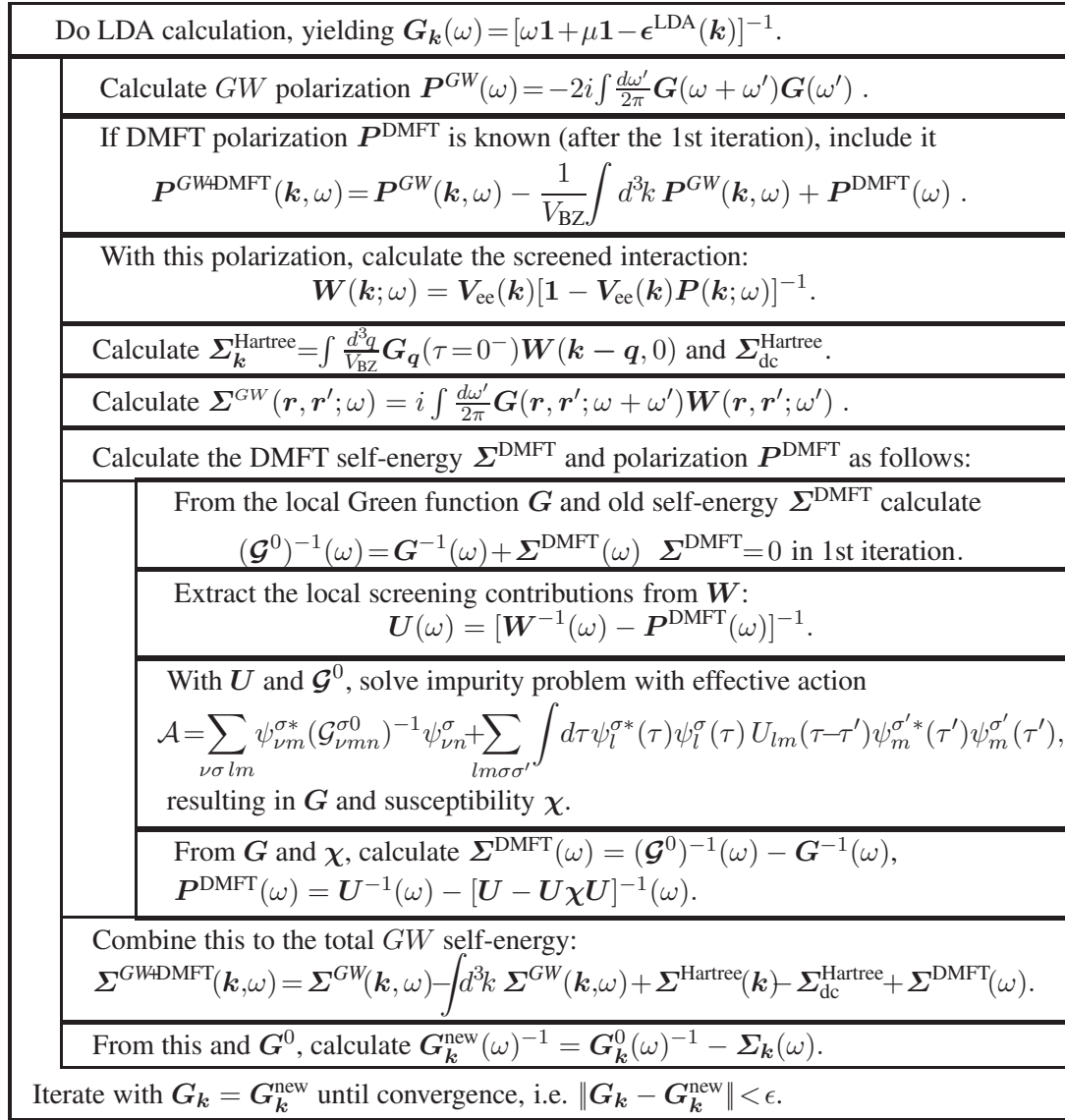
Fig. 15: *Flow diagram of the GW+DMFT algorithm (reproduced from [32]).*

in the first line of Fig. 15, where bold symbols denote an (orbital) matrix representation).

- From this Green function, the independent particle polarization operator P^{GW} is calculated convoluting two Green functions (2nd line of flow diagram Fig. 15). Note there is a factor of 2 for the spin.

- From the polarization operator in turn, the local polarization has to be subtracted since this can (and has to) be calculated more precisely within DMFT, which includes more than the RPA bubble diagram (after the first DMFT iteration).

- Next, the screened interaction W is calculated from the bare Coulomb interaction V_{ee} and the overall polarization operator $P^{GW+DMFT}$.

- Now, we are in the position to calculate the GW self energy. The first term is the Hartree

diagram, which can be calculated straight forwardly in imaginary time τ, yielding Σ^{Hartree} and the corresponding local contribution $\Sigma^{\text{Hartree}}_{\text{dc}}$, which we need to subtract later to avoid a double counting as it is also contained in the DMFT.

- The second diagram is the exchange from Fig. 1 which has the form G times W for the *GW* self energy.

- This *GW* self energy has to be supplemented by the local DMFT self energy, which together with the DMFT polarization operator is calculated in the following four steps:

  1. The non-interacting Green function $\mathcal{G}^0$ which defines a corresponding Anderson impurity model is calculated.

  2. The local (screened) Coulomb interaction $U(\omega)$ has to be determined *without* the local screening contribution, since the local screening will be again included in the DMFT. That is we have to "unscreen" W for these contributions.

  3. The Anderson impurity model defined by $\mathcal{G}^0$ and $U(\omega)$ has to be solved for its interacting Green function $G(\omega)$ and two-particle charge susceptibility χ. This is numerically certainly the most demanding step.

  4. From this $G(\omega)$ and $\mathcal{G}^0$, we obtain a new DMFT self energy $\Sigma(\omega)$ and from the charge susceptibility a new DMFT polarization operator.

- All three terms of the self-energy have now to be added; and the local screened exchange and Hartree contribution need to be subtracted to avoid a double counting.

- From this *GW*+DMFT self energy we can finally recalculate the Green function and iterate until convergence.

The flow diagram already shows that the *GW*+DMFT approach is much more involved than LDA+DMFT. However, it has the advantage that the double counting problem is solved and also the Coulomb interaction is calculated *ab initio* in a well defined and controlled way. Hence, no *ad hoc* formulas or parameters need to be introduced or adjusted.

For defining a well defined interface between *GW* and DMFT a particular problem is that *GW* is naturally formulated in real or **k** space and is presently implemented, e.g., in the LMTO [5] or PAW basis [20]. However, on the DMFT side we do need to identify the interacting *local d*- or *f*-orbitals on the sites of the transition metal or rare earth/lanthanoid sites, respectively. The switching between these two representations is non-trivial. It can be done by a downfolding [33, 34] or a projection onto Wannier orbitals, e.g., using maximally localized Wannier orbitals [35, 37] or a simpler projection onto the d (or f) part of the wave function within the atomic spheres [36, 38]. However, not only the one-particle wave functions and dispersion relation need to be projected onto the interacting subspace but also the interaction itself. To approach the latter, a constrained random phase approximation (cRPA) method has been proposed [39, 7] and improved by disentangling the d(or f)-bands [40]. The latter improvement now actually
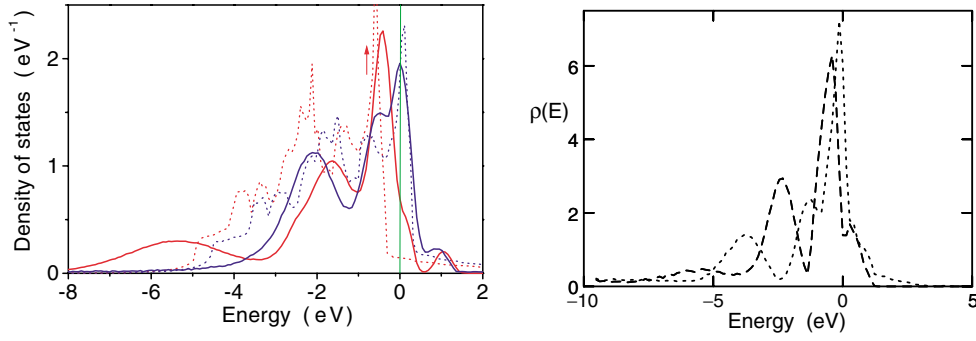
Fig. 16: *Spectrum (k-integrated) of Ni [left: LDA+DMFT (solid lines), spinpolarized LDA (LSDA) (dotted lines); right: GW+DMFT]. The two lines represent the minority- and majority-spin spectrum respectively. At roughly -6eV, a satellite peak is clearly visible in the majority-spin spectrum (reproduced from [26] and [27], respectively).*

allows us to do cRPA in practice. For the calculation of the two-particle polarization operators and interactions, Aryasetiawan *et al.* [41] even proposed to use a third basis: the optimal product basis.

On the DMFT side, the biggest open challenges are to actually perform the DMFT calculations with a frequency dependent Coulomb interaction $U(\omega)$ and to calculate the DMFT charge susceptibility or polarization operator.

As the fully self-consistent GW+DMFT scheme is a formidable task, Biermann *et al.* [27] employed a simplified implementation for their GW+DMFT calculation of Ni, which is actually the only GW+DMFT calculation hitherto: For the DMFT impurity problem, only the local Coulomb interaction between d orbitals was included and its frequency dependence was neglected $\mathbf{W}(\omega) \approx \mathbf{W}(0)$. Moreover, only one iteration step has been done, calculating the inter-site part of the self energy by GW with the LDA Green function as an input and the intra-site part of the self energy by DMFT (with the usual DMFT self-consistency loop). The GW polarization operator $\mathbf{P}^{\mathrm{GW}}$ was calculated from the LDA instead of the GW Green function. This is, actually, common practice even for conventional GW calculations which are often of the G_0W_0 form (see Section 3.2).

Fig. 16 (right panel) shows the GW+DMFT k-integrated spectral function of Ni which is similar to LDA+DMFT results (left panel). Both approaches yield a satellite peak at $\approx -6\,\mathrm{eV}$.

5   All of that: *ab intito* DΓA

From the Hedin equations, it seems to be much more natural to connect (i) the GW physics of screened exchange and (ii) strong, local correlations on the two-particle level than on the one particle level as done in GW+DMFT. In the Hedin equations, the natural starting point is the two-particle (particle-hole) irreducible vertex. A generalization of DMFT to n-particle correlation functions is the dynamical vertex approximation (DΓA) [42] which approximates the
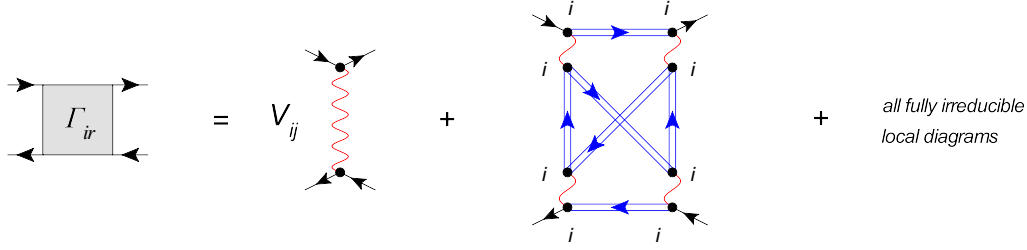
Fig. 17: *In* ab initio *DΓA we take as the fully irreducible vertex the bare Coulomb interaction plus all local vertex corrections (only one such diagram is exemplarily shown) [44].*

n-particle fully irreducible[8] vertex Γ_{ir} by the corresponding local contribution of all Feynman diagrams. For $n = 1$ the one-particle irreducible vertex is the self energy so that DΓA yields the DMFT. For $n = 2$, we obtain non-local correlations on all length scales and can calculate, e.g., the critical exponents of the Hubbard model [43].

Recently, some of us have proposed to use this DΓA *ab initio* for materials calculation [44]. The fully irreducible vertex Γ_{ir} is then given by the bare Coulomb interaction, which possibly is non-local, and all higher order local Feynman diagrams, see Fig. 17. From Γ_{ir} the full (reducible) vertex is calculated via the parqet equations [11]. The calculation of the local part of Γ_{ir} only requires us to calculate the two-particle Green functions of a single-site Anderson impurity model, which is well doable even for realistic multi-orbital models. For the parquet equations on the other hand, there has been some recent progress [45].

As a simplified version of *ab initio* DΓA one can restrict oneself to a subset of the three channels of the parquet equations, as was done in [42,43]. In this case one has to solve the Bethe-Salpeter equation with the particle-hole irreducible vertex Γ_{ph} instead of the parquet equations with the fully irreducible vertex Γ_{ir}. That is, our approximation to the Hedin equations is to take the local Γ_{ph}^* (all Feynman diagrams given by the local Green function and interaction) in the Hedin equation (8). In practice, one solves an Anderson impurity model numerically to calculate Γ_{ph}^*.

Full and simplified version of *ab initio* DΓA contain the diagrams (and physics) of GW, DMFT as well as non-local correlations which are responsible for (para-)magnons, (quantum) criticality and "all that".

Acknowledgment

---

[8]Fully irreducible means, cutting any two Green function lines does not separate the diagram into two parts. It is even more restrictive (less diagrams) than the particle-hole irreducible vertex (whose diagrams can be reducible e.g. in the particle-particle channel).

Appendices

A   Additional steps: equation of motion

In this appendix a detailed explanation is given how to derive the Hedin equation of motion for Σ, i.e., equation (16), from the standard equation of motion (15). In a first step Γ is expressed in terms of Γ^*. In order to keep the notation simple, the arguments of all functions are omitted and the functions are considered as operators.

The starting point of the calculations are the Bethe-Salpeter equations for Γ and Γ^*:

$$\Gamma = \Gamma_{\mathrm{ph}} + \Gamma\beta GG\Gamma_{\mathrm{ph}} \Longrightarrow \Gamma = \Gamma_{\mathrm{ph}}(1 - \beta GG\Gamma_{\mathrm{ph}})^{-1}$$
$$\Gamma^* = \Gamma_{\mathrm{ph}}^* + \Gamma_{\mathrm{ph}}^*\beta GG\Gamma^* \Longrightarrow \Gamma_{\mathrm{ph}}^* = \Gamma^*(1 + \beta GG\Gamma^*)^{-1}.$$
(24)

Using equation (10), i.e., $\Gamma_{\mathrm{ph}} = \Gamma_{\mathrm{ph}}^* + V$, one gets:

$$\Gamma = \left(\Gamma^*(1 + \beta GG\Gamma^*)^{-1} + V\right)\frac{1}{1 - \beta GG\left(\Gamma^*(1 + \beta GG\Gamma^*)^{-1} + V\right)}$$
(25)

Multiplying this equation with $1 = (1 + \beta GG\Gamma^*)^{-1}(1 + \beta GG\Gamma^*)$ and using the standard relations for operators, $A^{-1}B^{-1} = (BA)^{-1}$ leads to:

$$\Gamma = \left(\Gamma^*(1 + \beta GG\Gamma^*)^{-1} + V\right)\underbrace{V^{-1}V}_{1}\left(1 - \underbrace{(\beta GG + \beta GG\Gamma^*\beta GG)}_{P}V\right)^{-1}\left(1 + \beta GG\Gamma^*\right),$$
(26)

where $1 = V^{-1}V$ was inserted and the definition for the polarization operator, equation (7). Now one can use the second Hedin equation (6), which can be rewritten as $W = V(1 - PV)^{-1}$. Inserting this relation into the equation for Γ, one arrives at the following result:

$$\Gamma = \left(\Gamma^*(1 + \beta GG\Gamma^*)^{-1}\right)V^{-1}W\left(1 + \beta GG\Gamma^*\right) + W\left(1 + \beta GG\Gamma^*\right).$$
(27)

Another formulation of the second Hedin equation gives $V^{-1} = W^{-1} + P = W^{-1} + (1 + \beta GG\Gamma^*)\beta GG$. Replacing V^{-1} by this expression gives:

$$\Gamma = \Gamma^* + \Gamma^*\beta GGW(1 + \beta GG\Gamma^*) + W(1 + \beta GG\Gamma^*)$$
$$= \Gamma^* + \Gamma^*\beta GGW + \Gamma^*\beta GGW\beta GG\Gamma^* + W\beta GG\Gamma^* + W.$$
(28)

This equation shows how the full Γ is related to the Γ^*. Diagrammatically this relation is shown in Fig. 18.

In the next step Γ as given in equation (28) is inserted into equation (15), yielding

$$\Sigma = -GV\beta GG\Gamma - GV$$
$$= -GV\underbrace{(\beta GG + \beta GG\Gamma^*\beta GG)}_{P}W - GV\left(\underbrace{(\beta GG + \beta GG\Gamma^*\beta GG)}_{P}W + 1\right)\beta GG\Gamma^* - GV .$$
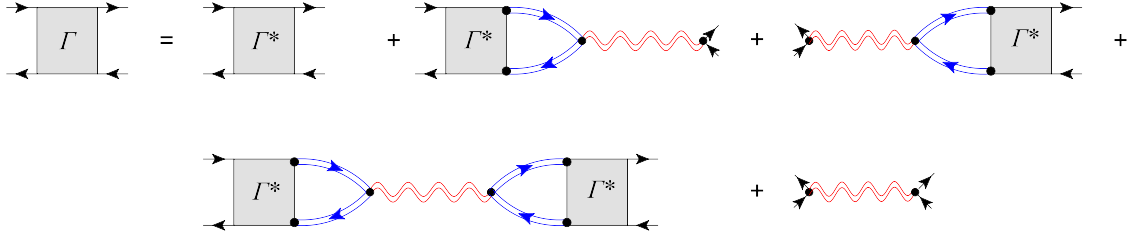(29)

Fig. 18: *Relation between Γ and Γ^* in terms of Feynman diagrams.*

From the second Hedin equation it follows that $VPW = W - V$. Inserting this relation into Equation (29) yields:

$$\begin{aligned}
\Sigma &= -G(W - V) - G(W - V)\beta GG\Gamma^* - GV\beta GG\Gamma^* - GV = \\
&= -GW - GW\beta GG\Gamma^*,
\end{aligned}$$

(30)

which is exactly equation (16).

Let us also, at this point, mention that Γ should satisfy an important relation:

$$\Gamma(11'; 22') = -\Gamma(12'; 21')$$

(31)

This relation is known as **crossing symmetry** (see e.g. [11], equation 7.5) and is simply a consequence of the Pauli-principle: Exchanging two identical fermions leads to a $-$ sign in the wave function. The screened interaction W, however, does not fulfill this crossing symmetry. Therefore, setting $\Gamma^* = 0$, as it is done in the GW-approximation leads to $\Gamma = W$ (see Fig. 18) which violates this crossing symmetry, i.e. it violates the Pauli-principle.

References

[1] P. Hohenberg and W. Kohn, Phys. Rev. **136** B864 (1964)

[2] R. O. Jones and O. Gunnarsson, Rev. Mod. Phys. **61** 689 (1989)

[3] See Lecture notes of P. Blöchl.

[4] L. Hedin, Phys. Rev. A **139** 796 (1965)

[5] For a review see, F. Aryasetiawn and O. Gunnarsson, Rep. Prog. Phys. **61** 237 (1998)

[6] A. A. Abrikosov, L. P. Gorkov and I. E. Dzyaloshinski, *Methods of Quantum Field Theory in Statistical Physics* (Dover, New York, 1963)

[7] For more details on RPA, see Lecture notes of F. Aryasetiawan

[8] W. Metzner and D. Vollhardt, Phys. Rev. Lett. **62** 324 (1989)

[9] A. Georges, G. Kotliar, W. Krauth and M. Rozenberg, Rev. Mod. Phys. **68** 13 (1996)

[10] For more details on DMFT, see Lecture notes of M. Kollar

[11] N. E. Bickers, "Self consistent Many-Body Theory of Condensed Matter" in *Theoretical Methods for Strongly Correlated Electrons CRM Series in Mathematical Physics Part III*, Springer (New York 2004)

[12] H. Jiang and R. Gomez-Abal and P. Rinke and M. Scheffler, Phys. Rev. Lett. **102**, 126403 (2009); Phys. Rev. B **82**, 045108 (2010)

[13] A. Stan, N. E. Dahlen, and R. van Leeuwen, J. Chem. Phys. **130**, 114105 (2009)

[14] C. Rostgaard, K. W. and Jacobsen, and K. S. Thygesen Phys. Rev. B **81**, 085103 (2010)

[15] W.-D. Schöne and A. G. Eguiluz, Phys. Rev. Lett. 81, 1662 (1998)

[16] A. Kutepov, S. Y. Savrasov, G. and Kotliar, Phys. Rev. B **80**, 041103 (2009)

[17] R. W. Godby, M. Schlüter and L. J. Sham, Pyhs. Rev. B **37** 10159 (1988)

[18] S. V. Faleev, M. van Schilfgaarde, and T. Kotani, Phys. Rev. Lett. **93**, 126406 (2004)

[19] A. N. Chantis, M. van Schilfgaarde, and T. Kotani, Phys. Rev. Lett. **96**, 086405 (2006)

[20] M. Shishkin and G. Kresse, Phys. Rev. B **74**, 035101 (2006)

[21] M. Shishkin, M. Marsman, and G. Kresse, Phys. Rev. Lett. **99**, 246403 (2007)

[22] I.-W. Lyo and W. E. Plummer, Phys. Rev. Lett. **60**, 1558 (1988)

[23] J. E. Northrup, M. S. Hybertsen, and S. G. Louie, Phys. Rev. Lett. **59** 819 (1987);
Phys. Rev. B **39**, 8198 (1989)

[24] S. Hüfner, G. K. Wertheim, N. V. Smith, and M. M. Traum,
Solid State Comm. **11** 323 (1972)

[25] F. Aryasetiawan, Phys. Rev. B **46**, 13051 (1972)

[26] A. I. Lichtenstein, M. I. Katsnelson, and G. Kotliar, Phys. Rev. Lett. **87** 67205 (2001)

[27] S. Biermann, F. Aryasetiawan, and A. Georges, Phys. Rev. Lett. **90** 086402 (2003)

[28] R. Keyling, W.-D.Schöne, and W. Ekardt, Phys. Rev. B **61**, 1670 (2000)

[29] P. H. Dederichs, S. Blügel, R. Zeller and H. Akai, Phys. Rev. Lett. **53** 2512 (1984)

[30] A. K. McMahan, R. M. Martin and S. Satpathy, Phys. Rev. B **38** 6650 (1988)

[31] O. Gunnarsson, O. K. Andersen, O. Jepsen and J. Zaanen, Phys. Rev. B **39** 1708 (1989)

[32] K. Held, Advances in Physics **56**, 829 (2007)

[33] O. K. Andersen, T. Saha-Dasgupta, R. W. Tank, C. Arcangeli, O. Jepsen and G. Krier, In
Lecture notes in Physics, edited by H. Dreysse (Springer, Berlin, 1999)

[34] O. K. Andersen, T. Saha-Dasgupta, S. Ezhov, L. Tsetseris, O. Jepsen, R. W. Tank and
C. A. G. Krier, Psi-k Newsletter **# 45** 86 (2001),
`http://psi-k.dl.ac.uk/newsletters/News_45/Highlight_45.pdf`

[35] N. Marzari and D. Vanderbilt, Phys. Rev. B **56** 12847 (1997)

[36] V.I. Anisimov, D.E. Kondakov, A.V. Kozhevnikov, I.A. Nekrasov, Z.V. Pchelkina, J.W.
Allen, S.-K. Mo, H.-D. Kim, P. Metcalf, S. Suga, A. Sekiyama, G. Keller, I. Leonov, X.
Ren, D. Vollhardt, Phys. Rev. B **71**, 125119 (2005)

[37] J. Kunes, R. Arita, P. Wissgott, A. Toschi, H. Ikeda, and K. Held, Comp. Phys. Comm.
181, 1888 (2010)

[38] M. Aichhorn, L. Pourovskii, V. Vildosola, M. Ferrero, O. Parcollet, T. Miyake, A. Georges,
and S. Biermann Phys. Rev. B **80**, 085101 (2009)

[39] F. Aryasetiawan, M. Imada, A. Georges, G, Kotliar, S. Biermann and A.I. Lichtenstein,
Phys. Rev. B **70**, 195104 (2004)

[40] T. Miyake, F. Aryasetiawan, M. Imada, arXiv:0906.1344

[41] F. Aryasetiawan, S. Biermann and A. Georges, In *Proceedings of the conference on "Co-
incidence Studies of Surfaces, Thin Films and Nanostructures"*, edited by A. Gonis
(Wiley, New York, 2004)

[42] A. Toschi, A.A. Katanin and K. Held, Phys. Rev. B 75, 045118 (2007);
      Prog. Theor. Phys. Suppl. 176, 117 (2008); Phys. Rev. B 80, 075104 (2009)

[43] G. Rohringer, A. Toschi, A.A. Katanin and K. Held arxiv.org/abs/1104.1919

[44] A. Toschi, G. Rohringer, A. A. Katanin, K. Held arxiv.org/abs/1104.2118

[45] S.-X. Yang, H. Fotso, J. Liu, T. A. Maier, K. Tomko, E.F. D'Azevedo, R.T. Scaletar,
      T. Pruschke, M. Jarrell, Phys. Rev. E 80, 046706 (2009)